Solar Energy 155 (2017) 1339–1353

Contents lists available at ScienceDirect

Solar Energy

journal homepage: www.elsevier.com/locate/solener

Geospatial analysis of the energy yield and environmental footprint of different photovoltaic module technologies

Atse Louwen [a,1], Ruud E.I. Schropp [b], Wilfried G.J.H.M. van Sark [a,*], André P.C. Faaij [c]

[a] Utrecht University, Copernicus Institute of Sustainable Development, Heidelberglaan 2, 3584CS Utrecht, The Netherlands
[b] Eindhoven University of Technology (TU/e), Applied Physics, P.O. Box 513, 5600MB Eindhoven, The Netherlands
[c] University of Groningen, Energy & Sustainability Research Institute, Blauwborgje 6, P.O. Box 9700 AE Groningen, The Netherlands

ARTICLE INFO

Article history:
Received 1 November 2016
Received in revised form 17 July 2017
Accepted 19 July 2017
Available online 5 August 2017

Keywords:
Photovoltaics
Performance
Geospatial
Environmental footprint

ABSTRACT

The majority of currently installed photovoltaic (PV) systems are based on mono- and polycrystalline silicon PV modules. Manufacturers of competing technologies often argue that due to the characteristics of their PV technologies, PV systems based on their modules are able to achieve higher annual energy yield, due to a smaller effect of temperature on module performance and/or a better performance at low light intensities. While these benefits have been confirmed in local studies many times, there is still limited insight as to the locations at which a particular technology actually performs best.

In this study we have analysed the performance of a large set of PV modules, based on irradiance time series that were taken from satellite measurements. Using these data, and combining it with a PV performance model, we have made a geospatial analysis of the energy yield of different types of PV modules. We aim to make the energy yield of the investigated modules spatially explicit, allowing PV system installers to choose the best module type for every location investigated. Our results show that there is large geographical variety in the performance of PV modules, in terms of energy yield but also in terms of relative performance or performance ratio. While some technologies clearly exhibit a decrease in performance ratio at locations where they operate at higher temperatures, for some technologies this effect is much smaller. As a result of the variation in performance, the environmental footprint of PV modules also shows large geographical variations. However, even at low irradiance locations the environmental footprint of PV modules in general is much lower compared to that of fossil fuel based electricity generation.

1. Introduction

The past decade saw exponential growth of installed photovoltaic (PV) solar energy system capacity. While at the end of 2005 cumulative global installed PV capacity was only around 5 GW_p, by the end of 2015, almost 230 GW_p of PV was installed (IEA PVPS, 2015, 2016; Louwen et al., 2016). The growth of installed capacity has been the result of increased demand due to incentive schemes, mainly by means of feed-in tariff systems in Germany and later China. Prices of PV modules (and systems) have dropped significantly over the last years, due to a variety of factors. First, production capacity across the PV supply chain has increased dramatically, resulting in over-supply of PV modules (Haegel et al., 2017). Secondly, technological innovation, resulting from both R&D and learning-by-doing, has improved PV production, resulting in for instance decreased consumption of silicon and silver, and increased module conversion efficiencies (ITRPV, 2017), thus lowering the price per unit of capacity.

The levelised cost of electricity (LCOE) from PV systems has dropped to values below that of conventional, fossil fuel based electricity production in some locations (Bloomberg, 2016). Furthermore, in many countries, PV electricity has achieved socket or grid parity. Examples are high irradiance countries like Spain, Cyprus and Israel, but also moderate and low irradiance countries like Italy, Germany, the Netherlands, Sweden and Denmark (Breyer and Gerlach, 2013). In many of these countries, there is even grid-parity for industrial electricity consumption (Breyer and Gerlach, 2013).

The majority (over 90%) of installed PV systems are based on PV modules made of either mono- or polycrystalline silicon (Fraunhofer ISE, 2016), while the remainder of systems are mostly based on PV modules made of cadmium telluride (CdTe) or

* Corresponding author.
E-mail addresses: a.louwen@uu.nl (A. Louwen), w.g.j.h.m.vansark@uu.nl (W.G.J.H.M. van Sark).
[1] Principal corresponding author.

http://dx.doi.org/10.1016/j.solener.2017.07.056
0038-092X/

copper-indium-gallium-selenium or copper-indium-selenium (CIGS or CIS) (Fraunhofer ISE, 2016; Jean et al., 2015). Other module technologies with small market shares are silicon heterojunction (SHJ) and thin-film amorphous silicon (a-Si). Manufacturers of technologies competing for market share with the incumbent crystalline silicon technologies often argue that their modules show superior energy yield in outdoor operation, due to better low-light performance (Solar Frontier, 2016) and/or lower temperature coefficient of module power (Solar Frontier, 2016; First Solar, 2016; Panasonic Corporation, 2016; Stion, 2016). For instance, while the performance of crystalline silicon modules normally decreases from its nameplate capacity with around 0.4% for every degree above 25 °C during operation, for SHJ modules this figure is normally below 0.3%/°C (Panasonic Corporation, 2016), and even lower for CdTe and a-Si modules (First Solar, 2016; KANEKA Solar Energy, 2016), due to differences in the band gap of the used semiconductor materials (Louwen et al., 2017). Due to these differences, manufacturers often argue that their technology will outperform conventional crystalline silicon modules in most locations, since modules will normally operate at temperatures that are significantly higher than the one at which nameplate capacity is determined (i.e. 25 °C).

In many PV performance studies, the benefits of the characteristics of these "alternative" technologies have been confirmed. For instance it was shown that SHJ modules achieve higher energy yield compared to crystalline silicon because of a lower detrimental effect of high operating temperatures (Zhao et al., 2013; Sharma et al., 2013; Zinsser et al., 2009). For a-Si and CdTe, this has also been established for certain locations (Sharma et al., 2013; Zinsser et al., 2009; Makrides et al., 2014). However, while we have information that in some specific cases one technology might outperform the other, there is limited information available that allows for an explicit comparison of the performance of different types of PV over broad geographical ranges. Furthermore, as the environmental impact of operation of PV systems is negligible (de Wild-Scholten, 2013; Fthenakis et al., 2011; Louwen et al., 2015), it follows that the environmental impact of PV electricity is defined by the ratio between environmental impact during all stages preceding and following PV system operation and the lifetime energy yield. These phases, including extraction of raw materials, manufacturing, and end-of-life treatment, result in a fixed environmental impact per unit of PV system nameplate capacity, regardless of how or where the system operates. Thus, the environmental impact per unit of electricity produced with PV systems is largely dependent on the annual yield an thus will show large geographical variation. Recently, a web client was released that aims to show this geographical variation of environmental impact (Pérez-López et al., 2016). Although this web client presents results for a large number of technologies, both current and prospective, it does not include detailed modelling of PV performance, but rather calculates energy yield based on a user-determined performance ratio and average annual insolation figures.

Therefore, in this study we aim to use detailed modelling of the energy performance of different PV module technologies to determine the geospatial variation in performance of PV, in terms of energy yield, energy yield relative to that expected from the nameplate capacity (performance ratio), and environmental performance. The results should offer insights in which technology performs best at which location, in terms of these several criteria, and can be used by system installers, investors and policy makers to make sound decisions on choosing technology types for a specific location.

2. Methods

For this study, we used irradiance, air temperature, and wind speed measurements from satellite measurements to model the performance of different types of PV modules. First we used the irradiance time series to calculate the optimum tilt of the PV module array for every location in our analysis. Then, we modelled plane-of-array irradiance time series for these tilted planes, and used these plane-of-array time series to model PV power output and energy yield. The resulting data was used to model energy yield and performance ratio (*PR*). Finally, the energy yield was used to calculate energy payback time (EPBT), greenhouse gas (GHG) emission factor(gCO_2-eq/kW h), and GHG payback time (GHGPBT). These impacts were calculated based on data from previously published life cycle assessment studies and data on energy efficiency and GHG footprints of country-level electricity mixes. All results are presented for a broad geographical scope.

2.1. Irradiance and weather data

We obtained global horizontal irradiance time series with a temporal resolution of 15 min, and a geographical resolution of 0.5° by 0.5°, from measurements of the HelioClim irradiance database (version HelioClim-3v5), for the year 2005 (SoDa, 2016). We also obtained wind speed and temperature measurements with the same geographical resolution, and a temporal resolution of 6 h (European Centre for Medium-Range Weather Forecasts, 2016). The two datasets were combined by linearly interpolating the wind speed and temperature measurements to a 15 min resolution. This combination strategy means the weather data inputs are based on 6-h averages, minimising extreme values in ambient temperature and wind speeds, which affects the model results. However, irradiance generally varies much more on a daily basis compared to air temperature and wind speed, and PV power is much more strongly affected by irradiance than by temperature (Hansen et al., 2012). Furthermore, for our location in Utrecht, the Netherlands, comparison of the model results with high and low temporal resolution weather-data shows that the difference in modelled annual yield is on average (for all studied modules) less than 0.2%. Thus, we assume the effect of the low temporal resolution weather data on the model accuracy to be limited for all locations. The geographical scope of the data includes most of Europe, all of Africa, and the Middle-East.

2.2. Optimum tilt and plane-of-array irradiance

The global horizontal irradiance (GHI) data was converted to plane-of-array (POA) irradiance time series using the Hay-Davies model (Hay and Davies, 1980), which calculates POA irradiance from global horizontal irradiance (GHI), direct normal irradiance (DNI), diffuse horizontal irradiance (DHI) and extraterrestrial DNI. The DNI was calculated from the GHI using the DIRINT model (Ineichen et al., 1992). The extraterrestrial DNI was calculated according to (Paltridge and Platt, 1976; Duffie and Beckman, 2013). The beam component of the GHI was calculated from DNI for a horizontal plane to establish the diffuse horizontal irradiance (DHI). The optimum POA tilt was assumed to be the tilt at which the annual POA irradiance is at its maximum. Here, we assume the optimal orientation of the surface of the PV modules to be towards the equator, e.g. due south in the northern hemisphere, due north in the southern hemisphere. The POA irradiance was calculated in several iterations for every location, until a maximum was found. The determination of optimum tilt was performed with irradiance time series downsampled to hourly resolution to reduce computation time. The resulting optimum tilt was used to calculate 15 min POA time series using the previously described approach. The dataflow for the determination of optimum tilt is shown in Fig. D.1. The resulting optimum tilts and plane-of-array irradiance sums are shown in Fig. 1, in which it is shown that the optimum tilt varies from 0 ° near the equator to roughly 45°

at the highest latitudes. The figure furthermore shows that there is as expected a large, predominantly latitudinal, variation of POA insolation, with POA insolation ranging from under 1000 kW h m^{-2} y^{-1} to over 2500 kW h m^{-2} y^{-1}. Considering that we only use a dataset for one year (2005), we compared our results with those from PVGIS,[2] showing very similar results for a typical meteorological year.

2.3. PV performance modelling

The POA irradiance time series obtained in the previous step are comprised of global, direct, sky diffuse and ground diffuse irradiance in the plane-of-array. These datasets are used as input in the PVLIB-python implementation (Holmgren et al., 2015) of the Sandia Array Performance Model (SAPM). SAPM was developed by Sandia National Laboratories and models the performance of PV modules based on module specifications, direct and diffuse POA irradiance, cell temperature, airmass and angle-of-incidence of the direct irradiance on the module plane (King et al., 2004). Aside from the normally listed modules specifications, the model uses empirically determined module coefficients that take into account the effects of airmass and angle-of-incidence on module performance. The effects of these parameters was established for a wide range of modules by performing a fit of a polynomial model. The dataflow of the PV performance model is shown in the Appendix in Fig. D.1.

The cell temperature is calculated based on an empirical model also developed by Sandia National Laboratories which is included in the PVLIB-python SAPM implementation. It takes into account total POA irradiance, ambient temperature, wind-speed, and the type of module backside (glass, polymer, steel) and the type of installation (open-rack, roof-mounted, etc.). For this study we use the roof-mounted setting, as we investigate the environmental performance of PV systems based on an LCA study of roof-mounted PV systems (see also Section 2.5).

The output of the SAPM model is a time series of the direct-current (DC) characteristics of the modelled module, and includes short-circuit current (I_{sc}), maximum power current (I_{mp}), open-circuit voltage (V_{oc}), maximum power voltage (V_{mp}), and maximum power point power (P_{mpp}).

2.4. Annual energy yield and performance ratio

The SAPM time series are used to establish the performance of the modelled PV modules on an annual basis. The annual energy yield is calculated from the time series as:

$$E_{annual} = \sum_{t=0}^{y} P_{mpp}(t) \cdot \eta_{inv}(P_{mpp}) \cdot \Delta t \cdot f_{deg} f_{loss} \quad (1)$$

where E_{annual} is the annual energy yield and Δt is the time step between measurements (15 min). Inverter efficiency is modelled here as η_{inv}, based on the PV load profiles. The factor f_{deg}, describing module degradation, was calculated for the PV system lifetimes of 30 years, based on a degradation rate of 0.67% per year (20% degradation in 30 years) for all technologies, thus f_{deg} amounts to 0.9. Reported linear degradation rates in Jordan et al. (2016) are 0.5%/yr for crystalline silicon and CIGS technologies, 1%/yr for thin film silicon and SHJ technologies. However, even though this study by Jordan et al. is (one of) the most comprehensive overviews of degradation rates in PV technologies, data availability varies per technology, both in sample size and time horizon. Furthermore, especially CdTe exhibits non-linear degradation modes, which are not fully understood at the moment. Therefore, we assume an equal degradation rate for all technologies based on the IEA PVPS Task 12 LCA recommendations (Frischknecht et al., 2016) as it said to reflect the warranties most PV manufacturers give.

The factor f_{loss} describes the effect of assumed system losses for soiling, module mismatch, wiring and connection resistance, and light-induced degradation. Table 1 shows an overview of the loss-parameters included here. Total system losses are estimated to be 6.8%, thus f_{loss} is estimated at 93.2%. The losses presented in Table 1 are dependent on the module characteristics, PV-module string layout, type of inverter, length of cabling, etc. Soiling losses are furthermore very much dependent on location, as for instance precipitation amount and frequency and dust loading of the local environment determine average soiling losses (García et al., 2011). We have tried to identify typical values for the parameters shown, however, they are included here primarily to offer a somewhat rough indication of typical system losses, and to account for these losses in calculating the environmental impacts. Because our primary aim was to compare different PV technologies, inverter efficiency, degradation and loss factors were assumed to be equal for all technologies, to exclude any influence of these parameters on the AC power that can be fed into the grid.

The performance ratio (*PR*) is defined as the ratio between the actual energy yield E_{annual} and the reference yield, the yield that is expected when we take only into account the rated power of the PV module (P_{STC}) and the annual insolation at the module plane (van Sark et al., 2012; IEC TS 61724-3:2016, 2016). It is calculated for each module type as:

$$PR_{AC} = \frac{E_{annual}}{P_{STC} \cdot H_{POA,annual} \cdot (G_{STC})^{-1}} \quad (2)$$

where $H_{POA,annual}$ is the insolation (annual irradiance sum) at the POA, and G_{STC} is the STC irradiance at which the P_{STC} is determined. The *PR* is normally calculated for actually measured energy yield, but here we calculate it using the modelled annual energy yield of the PV modules and the assumed loss factors.

2.5. Environmental indicators

The annual energy yield of PV modules is of course very important for investment decisions, but it also determines the environmental impact of PV (Frischknecht et al., 2016). The environmental impact of PV systems is normally established in life cycle assessment (LCA) studies, for which data are gathered, in a life cycle inventory, that cover all material and energy flows occurring during the complete life cycle of a product (e.g. from raw material production to operation and end-of-life treatment). The resulting life cycle inventory is then used to attribute environmental impact to PV systems and electricity produced with them. Most commonly for PV systems, the impact in terms of energy demand and greenhouse gas emissions is reported. The general methodology for performing LCA studies is standardised by the ISO (ISO 14040:2006, 2006; ISO 14044:2006, 2006), and the IEA Photovoltaic Power Systems Programme has also developed methodology guidelines specifically for PV systems (Frischknecht et al., 2016). Here, we analyse the geospatial variation of three environmental impact indicators, energy payback time (EPBT), life-cycle greenhouse gas (GHG) emissions and GHG payback time (GHGPBT), which were previously reported in (amongst many other studies) (Louwen et al., 2015; de Wild-Scholten, 2013; Frischknecht et al., 2016; Leccisi et al., 2016; Wetzel and Borchers, 2014).

The EBPT is defined as the time it takes for a PV system to produce the same amount of energy that is consumed during its whole life cycle. For PV systems, most of the energy is consumed during

[2] http://re.jrc.ec.europa.eu/pvgis.

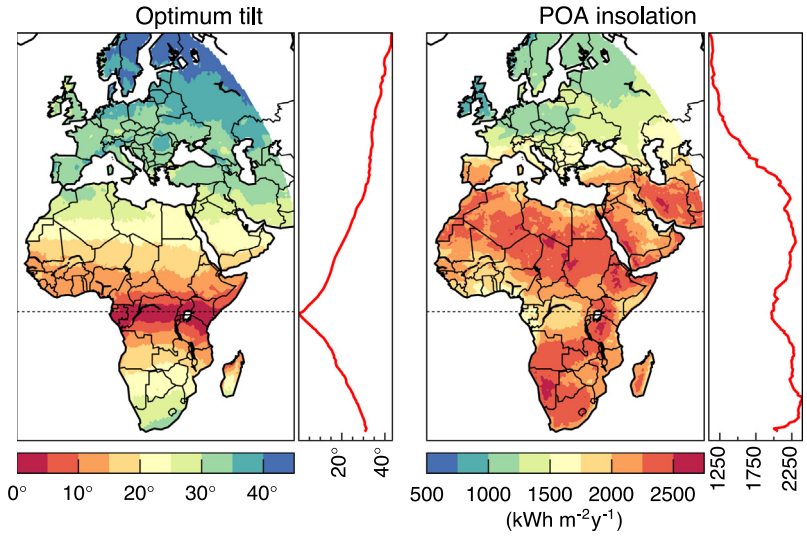

Fig. 1. Global optimum plane-of-array (POA) tilts and POA insolation for optimally tilted surfaces, calculated from global horizontal irradiance time series for the year 2005, converted to POA using the Hay-Davies model. The curves on the right side of the map indicate average tilt and POA insolation as a function of latitude.

Table 1
Overview of loss factors of PV systems assumed in this study for the calculation of annual energy yield.

Loss parameter	Losses	Source
Soiling	2.0%	Typical value assumed in Dobos (2014)
Module mismatch	1.71%	Picault et al. (2010)
Wiring losses	1.25%	Reich et al. (2012)
Connection losses	0.5%	Typical value assumed in Dobos (2014)
Light-induced degradation	1.5%	Typical value assumed in Dobos (2014)
Total combined losses	6.78%	

the manufacturing of its components (Leccisi et al., 2016; Frischknecht et al., 2016; Louwen et al., 2015; de Wild-Scholten, 2013). In general, the EPBT is calculated as Frischknecht et al. (2016):

$$EPBT = \frac{E_{prod} + E_{tran} + E_{inst} + E_{EOL}}{E_{annual} \cdot f_{deg} \cdot f_{loss} \cdot \eta_{inv} \cdot (\eta_G)^{-1}} - E_{OM} \quad (3)$$

where the terms in the numerator are the energy invested for production (E_{prod}), transport (E_{tran}), installation (E_{inst}), and end-of-life treatment (E_{EOL}). E_{OM} is the energy invested during operation and maintenance. All these parameters are expressed in MJ of primary energy (MJ_P). The installation, operation, and maintenance activities do not contribute substantially to the overall cumulative energy demand of a PV system's lifecycle (Jungbluth et al., 2009; Wernet et al., 2016)and are thus neglected. Furthermore, end-of-life treatment is not included in our analysis. Including end-of-life treatment would likely not increase the life cycle cumulative energy demand or other environmental impacts, as the recycling of especially aluminium and silicon were shown to have environmental benefits (Leccisi et al., 2016; Corcelli et al., 2016).

The parameter η_G is the primary energy to electricity conversion efficiency for the grid where the PV system is installed (Frischknecht et al., 2016). As described in the *Methodology Guidelines on Life Cycle Assessment of Photovoltaic Electricity* (Frischknecht et al., 2016), there are two main options for determining the value of η_G: first, by assuming the installed PV systems electricity production replaces the average grid mix of electricity at the point of installation (total EPBT, e.g including renewable and non-renewable energy sources) and secondly, by assuming the installed PV system replaces only non-renewable electricity at the point of installation (non-renewable EPBT). In terms of capacity additions and decommissioning, there is support to assume the latter, as the newly installed capacity is mainly in the form of renewable electricity, while the capacity that is decommissioned is likely mostly non-renewable. However, considering the intermittent nature of electricity production from PV one could also argue that at the time of generation PV is more likely to replace flexible electricity supply, like natural gas fired power plants, especially at high PV penetration levels and in the absence of sufficient flexible storage capacity or demand response. In this study we analyse and present both the total EPBT as well as the non-renewable EPBT. The difference between the total and non-renewable EPBT depends on the penetration level of renewable electricity sources. In countries with very high shares of renewable energy (mainly hydropower) like Norway, there will be a big difference between the two, while in at low penetration levels or renewable electricity, the difference will be small. In Fig. 2 we indicate the difference between total and non-renewable EPBT for two countries (Norway and the Netherlands) and for the average grid efficiencies in our dataset. For the average grid efficiencies, the difference between total and non-renewable EPBT is about 30%.

For η_G we take country average values where available, otherwise we take values for a larger geographical scope. The energy demand for production of the various types of PV was taken from recent life cycle assessment (LCA) studies (de Wild-Scholten, 2013; Louwen et al., 2015). In the study by De Wild-Scholten (de Wild-Scholten, 2013), all investigated PV technologies are studied except for SHJ systems. The results are based on recent data from PV manufacturers combined with existing life cycle inventories from the ecoinvent 2.2 database (Jungbluth et al., 2009). The life cycle data for SHJ systems was taken from our own study (Louwen et al., 2015), which is also based on ecoinvent 2.2 data, with updates for processes specific for SHJ cell and module production. The results presented in the study are calculated for roof-top mounted systems. We used the results expressed per unit of rated capacity for our calculations, so other considerations in the LCA studies that influence lifetime energy yield do not affect our results. In terms of manufacturing location, we assume 65% of PV manufacturing to take place in China and 35% outside of China, based on Fraunhofer ISE (2016). We thus calculated a market average environmental impact from the results in de Wild-Scholten (2013) and

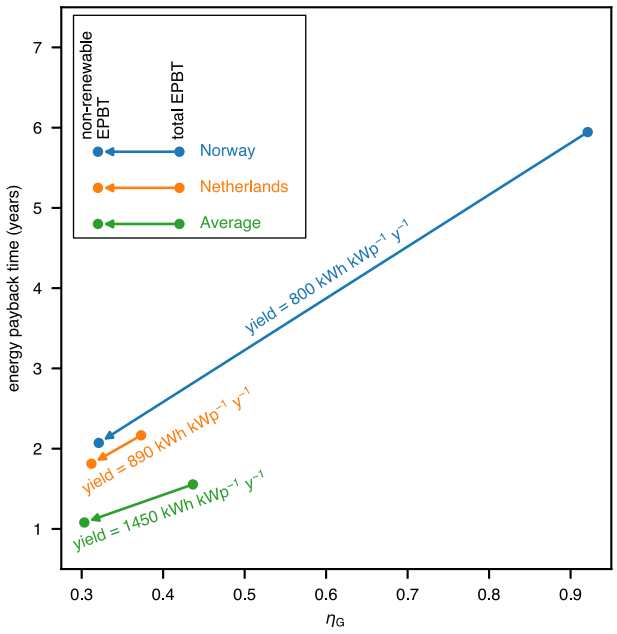

Fig. 2. Example of the difference between total and non-renewable EPBT for grid efficiency values of Norway and the Netherlands, and the overall average grid efficiency. The values are calculated with the indicative yield figures show in the chart, for silicon heterojunction PV systems.

Louwen et al. (2015), making the rough assumption that production in Europe as reported in these studies is characteristic for production outside of China.

The greenhouse gas (GHG) emissions of PV electricity are normally expressed per kW h of electricity generated with a PV system. It is calculated by summing all the CO_2-eq emissions that originate during production, transport, installation, operation and end-of-life treatment of the PV system and dividing this figure by the lifetime energy output of the PV system.

To analyse the geospatial distribution of GHG emissions from PV, we took life cycle GHG emissions data for the studied module technologies from the previously mentioned LCA studies(de Wild-Scholten, 2013; Louwen et al., 2015). From these studies, we established the GHG emissions related with producing a PV system expressed per unit of PV system capacity (gCO_2-eq/W_p). The yield figures modelled here where then used to calculated a GHG emission factor (gCO_2-eq/kW h):

$$G_{elec} = \frac{G_{prod} + G_{tran} + G_{inst} + G_{EOL}}{E_{annual} \cdot f_{deg} \cdot f_{loss} \cdot \eta_{inv} \cdot T_{life}} \quad (4)$$

where G_{elec} is the GHG emission factor in gCO_2-eq/kW h, $G_{prod}, G_{tran}, G_{inst}$ and G_{EOL} are the GHG emission associated with production, transportation and installation and end-of-life treatment of a PV system, respectively, E_{annual} is the annual energy production (which we model here), T_{life} is the expected lifetime of the system (assumed to be 30 years for all module types). Note that as for EPBT, installation, operation and maintenance, and end-of-life treatment are neglected here.

Similar to EPBT, we also calculate the time in which the GHG emissions released during the various stages of the PV systems' life cycles are payed back by replacing electricity produced from the average electricity grid, the GHG payback time (GHGPBT). The GHGPBT is calculated similar to EPBT (Frischknecht et al., 2016) as:

$$GHGPBT = \frac{G_{prod} + G_{tran} + G_{inst} + G_{EOL}}{E_{annual} \cdot f_{deg} \cdot f_{loss} \cdot \eta_{inv} \cdot (G_{gridavg} - G_{elec})} \quad (5)$$

where $G_{gridavg}$ is the country average grid GHG emissions factor. This factor was calculated by combining GHG emission data from World Resources Institute (2015) and electricity production data from United Nations Statistics Division (2015). For countries where data is missing, or where the GHG emission factor is above the 95th percentile of all countries analysed, we assume the average value for all countries. For a list of those countries please see the appendix.

It is to be noted that the GHG emission factor G_{elec} and the GHGPBT we show below do not represent point-of-generation GHG emissions, but rather represent what emission can be attributed to PV produced elsewhere, when installed in each location shown on the maps. Thus, the emissions from PV production are associated with a fixed production location, and the variation in G_{elec} comes from the variation of performance of PV at different locations. Furthermore, for GHGPBT we assume a grid emission factor that is constant within each country. Especially for larger countries, the shown GHGHPBT does not necessarily reflect local conditions. The results are thus considered to be indicative, but shown nonetheless, to indicate that the energy yield of PV at different locations can result in significant variation in G_{elec} compared to the results obtained in LCA studies that assume a specific energy yield of (normally) 1275 kW h kW_p^{-1} y^{-1} (Alsema et al., 2009; Fthenakis et al., 2011; Frischknecht et al., 2016). We also aim to show indicatively how the combination of local attainable energy yield from PV and local grid emission factors results in the ability of PV to contribute to decarbonisation of electricity generation.

2.6. Selection of studied modules and comparison of PV technologies

In this study we analyse six different PV technologies: SHJ, mono-Si, poly-Si, CdTe, CI(G) S, and tandem a-Si. For each PV technology we have analysed eight different, recent PV modules for which we were able to obtain the SAPM performance coefficients. We present our results per technology, by taking the average result for the studied modules. For all PV technologies, we assume that each of the eight modules are integrated in a roof-top mounted system to model annual energy yield. Here, we are taking into account typical DC and AC yield losses and PV module degradation (see also Section 2.4 and Table 1). For each module technology we also investigate the variation in the obtained results between the eight modules selected per technology. The variation is calculated per location as the relative standard deviation of all eight model results at this location, by dividing the absolute standard deviation by the mean result at each location.

3. Comparison of PV module technologies

The results of our modelling analyses are shown in Figs. 3–7 for energy yield, performance ratio, energy payback time, GHG emission factor, and GHG payback time. Fig. 3 shows the annual energy yield of SHJ modules, and the relative yield of SHJ modules compared to modules of 5 other types of PV. The results indicate that the SHJ technology outperforms the other technologies in most locations except for the CdTe technology. The results for the mono- and especially the poly-Si modules furthermore indicate that the yield advantage of SHJ modules becomes larger in locations closer to the equator, likely due to higher operating temperatures and the smaller effect of higher temperature on SHJ's performance. The yield of PV systems, calculated from modelled DC performance taking into account degradation, loss factors, and inverter efficiency as described in Section 2.4, ranges from around 600 kW h kW_p^{-1} y^{-1} in locations with low irradiance to around 2000 kW h kW_p^{-1} y^{-1} in high-irradiance locations. Fig. 4 shows the performance ratio of the studied PV systems. Taking into account the losses described in Section 2.4, the *PR* ranges from under 60% to around 85% over all technologies. As *PR* is essentially

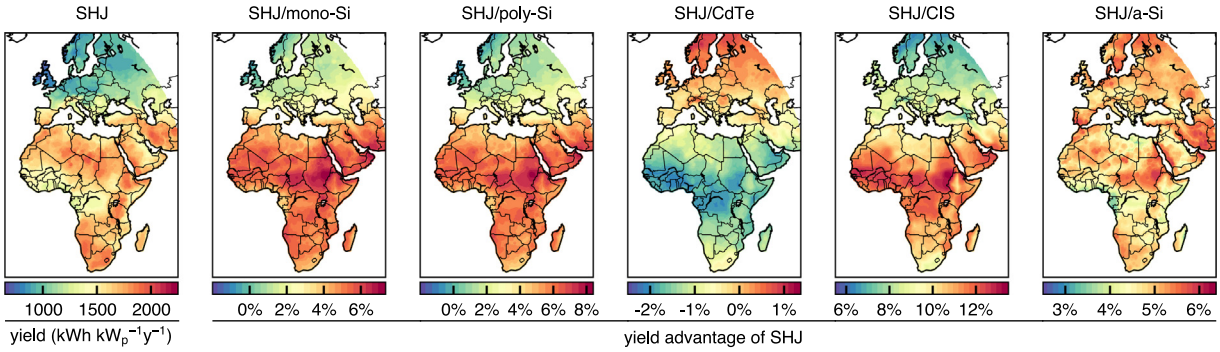

Fig. 3. Overview of the modelled annual energy yield of optimally tilted PV systems in kW h/kW$_p$ (SHJ) and relative yield of SHJ compared to other technologies for the year 2005, calculated with the Sandia Array Performance Model (King et al., 2004) using 15-min resolution plane-of-array irradiance time series (SoDa, 2016) and 6-h ambient temperature and wind-speed time series (European Centre for Medium-Range Weather Forecasts, 2016).

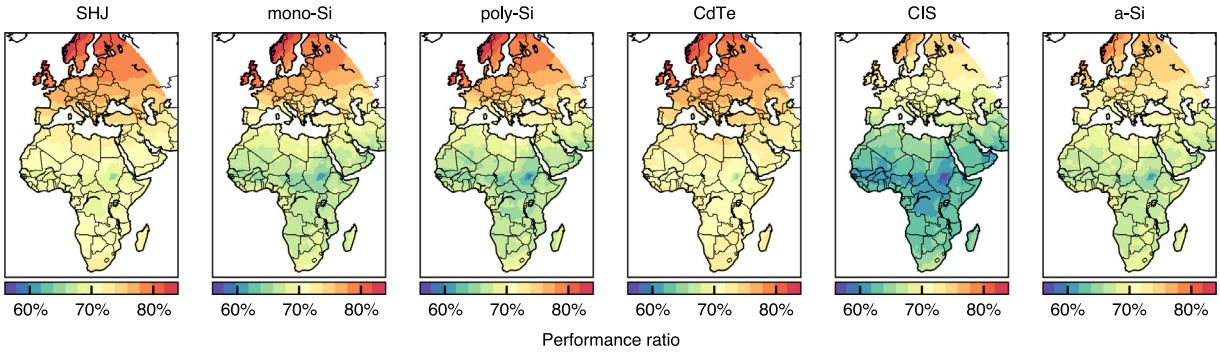

Fig. 4. Overview of the modelled annual performance ratio (PR_{AC}) of optimally tilted PV modules of the six module technologies, for the year 2005, calculated with the Sandia Array Performance Model (King et al., 2004) using 15-min resolution plane-of-array irradiance time series (SoDa, 2016) and 6-h ambient temperature and wind-speed time series (European Centre for Medium-Range Weather Forecasts, 2016).

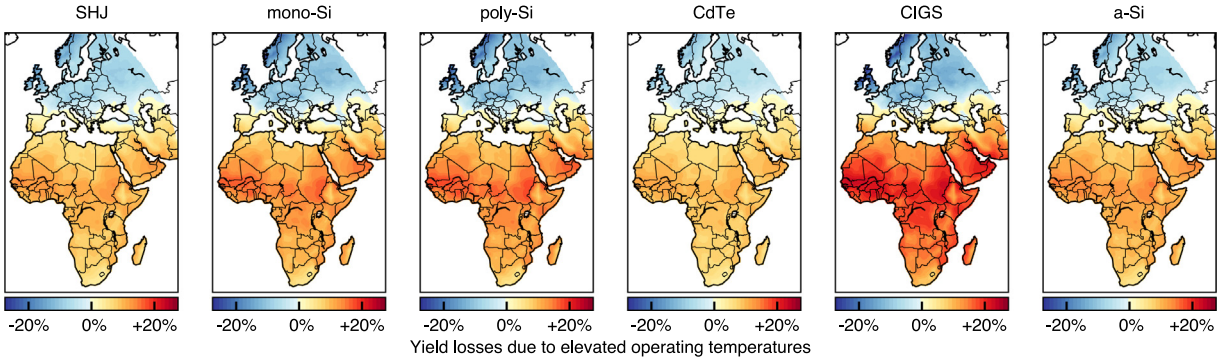

Fig. 5. Overview of the modelled relative temperature related yield losses for the year 2005, calculated with the Sandia Array Performance Model (King et al., 2004) using 15-min resolution plane-of-array irradiance time series (SoDa, 2016) and 6-h ambient temperature and wind-speed time series (European Centre for Medium-Range Weather Forecasts, 2016). Note that negative yield losses indicate yield gains due to low operating temperatures.

energy yield corrected for irradiance, Fig. 4 more clearly shows the latitudinal variation of performance. For most technologies the main variation in *PR* is a result of variations in operating temperature. Fig. 5 shows the effect of temperature on annual PV yield. Comparing with Fig. 4, it indicates that the decrease of *PR* at low latitudes can largely be attributed to temperature related yield losses. Temperature related yield losses vary per technology, and are highest for the CIGS modules for which they exceed 22% in locations with high irradiance and temperature. For other technologies, temperature related yield losses are still significant in these locations at around 17% for crystalline silicon technologies, over 14% for thin-film silicon, over 13% for SHJ and over 11% for CdTe. Temperature related *gains* in cold, low-irradiance locations show a similar trend, over 22% for CIGS, 18–19% for crystalline silicon, 13–14% for SHJ and a-Si, and 10% for CdTe.

Fig. 6 shows that the energy payback time of PV modules shows large variation, not only from high to low latitudes, but also from one country to the other. This is due to the fact that EPBT is calculated using the country average grid efficiency. Countries with high shares of renewable electricity (especially hydropower) with high primary energy to electricity conversion efficiency show high payback times. Norway is a notable example of this phenomenon, not only because of the low irradiance, but because a very large fraction of the electricity produced there is from hydropower. Another notable example is the DR Congo, which also has a high share of hydropower in its electricity supply, and as a result shows high

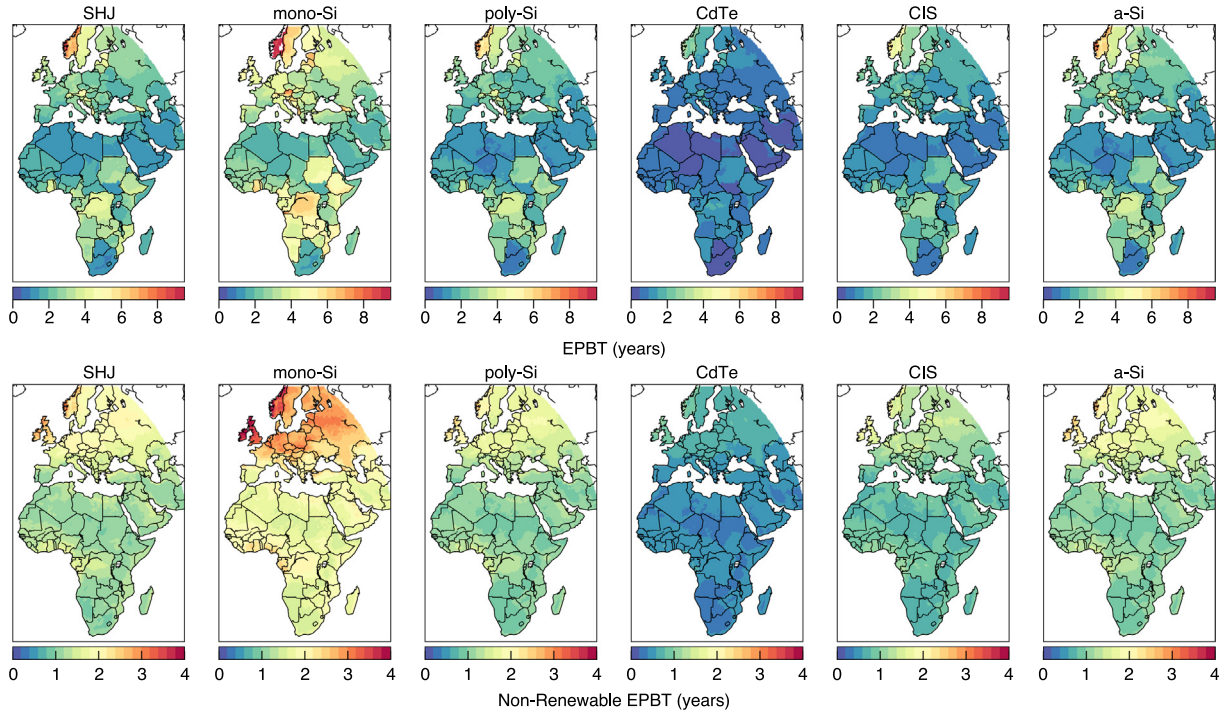

Fig. 6. Overview of the modelled energy payback time (EBPT) and non-renewable EPBT of optimally tilted PV systems in years, calculated with the Sandia Array Performance Model (King et al., 2004) using 15-min resolution plane-of-array irradiance time series (SoDa, 2016) and 6-h ambient temperature and wind-speed time series (European Centre for Medium-Range Weather Forecasts, 2016) for 2005.

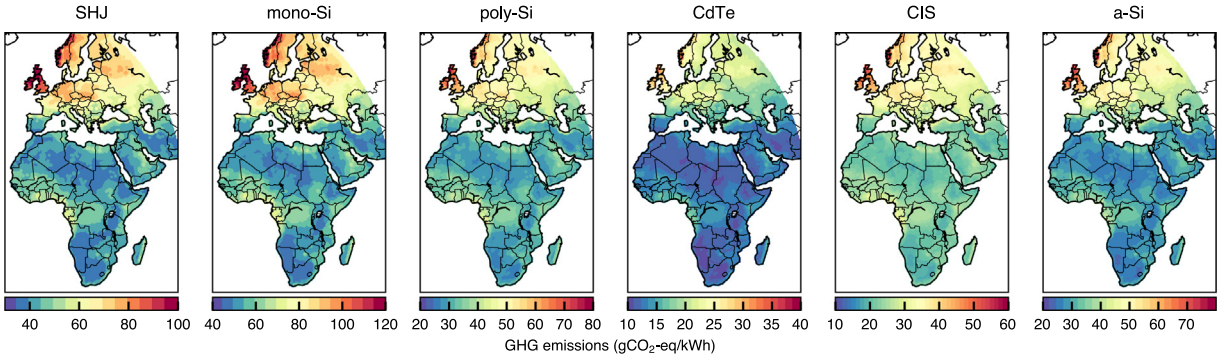

Fig. 7. Overview of the modelled greenhouse gas emission factor of optimally tilted PV systems in gCO_2-eq/kW h, calculated with the Sandia Array Performance Model (King et al., 2004) using 15-min resolution plane-of-array irradiance time series (SoDa, 2016) and 6-h ambient temperature and wind-speed time series (European Centre for Medium-Range Weather Forecasts, 2016) for 2005.

EPBT even though PV yields are quite high. The bottom row of Fig. 6 shows the non-renewable EPBT. There is less variation in the nrEPBT from country to country, thus, the geographical variation in nrEPBT more closely resembles the geographical yield variations shown in Fig. 3. Non-Renewable EPBTs are below 4 years for all technologies and locations.

CdTe based systems show the lowest EPBT, which is below 0.5 years in many locations, especially on the African continent, but even in some southern European locations. Although SHJ modules show higher yield compared to poly-Si, CIGS and a-Si, the latter have lower EPBT in most locations due to a much lower energy consumption for manufacturing. Mono-Si systems, with the highest energy demand for manufacturing, relatively have the highest EPBT in all locations.

The GHG emission factors and GHGPBT are shown in Figs. 7 and 8, respectively. Fig. 7 shows that for very large geographical ranges the GHG emissions factors of all module technologies are around or below 50 gCO_2-eq/kW h. For CdTe modules, large areas even show emission factor around or below 15 gCO_2-eq/kW h, while the monocrystalline silicon devices show the highest GHG emission factors per kW h. This is mainly due to the fact that CdTe modules have lower GHG emissions from manufacturing and high energy performances compared to other technologies, and that mono-Si modules have the highest GHG emissions. The highest GHG emissions per kW h are thus those associated with mono-Si modules in areas with low insolation, and are around or below 120 gCO_2-eq/kW h, and thus well below fossil fuel alternatives, even those equipped with carbon-capture-and-storage (CCS) systems. For conventional fossil fuelled electricity generation, the GHG emissions range from roughly 400 to over 1000gCO_2-eq/kW h,depending on the fuel type and without CCS. For most locations and technologies the emission factor of PV is around or well below 60 gCO_2-eq/kW h.

Fig. 8 shows that there is large variation in the GHGPBT. For countries with high grid emission factors, the GHG PBT can be very

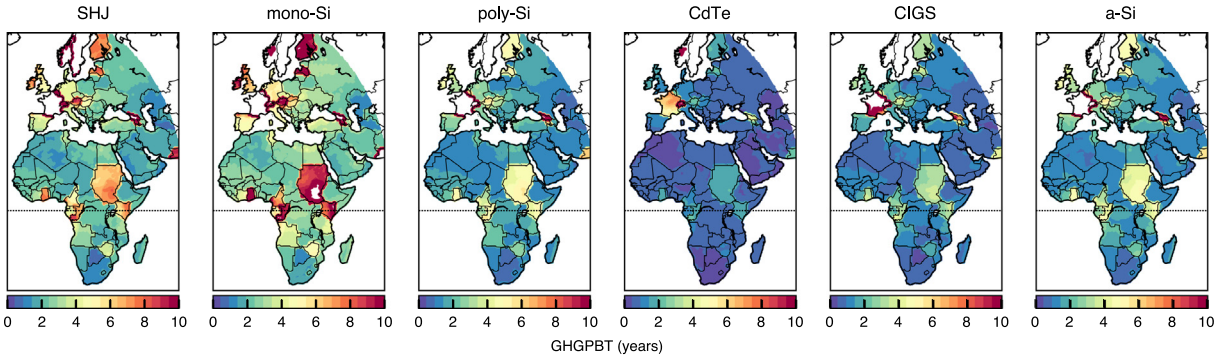

Fig. 8. Overview of the modelled greenhouse gas emission payback time (GHGPBT) of optimally tilted PV systems in years, calculated with the Sandia Array Performance Model (King et al., 2004) using 15-min resolution plane-of-array irradiance time series (SoDa, 2016) and 6-h ambient temperature and wind-speed time series (European Centre for Medium-Range Weather Forecasts, 2016) for 2005. The white areas in the graph indicate locations where the GHGPBT exceeds 10 years.

short (below 2 years). Especially for lower latitude countries and for CdTe systems, the GHGPBT can be below 0.5 years. Some countries with low grid-average GHG emission factors (e.g. France, Norway and Sweden) show GHGPBT over 10 years, as the difference with the GHG emission factor of PV electricity is in these cases very small. This is due to high shares of hydropower (Norway) or nuclear energy (France, Sweden). Because of its very low GHG footprint, CdTe still shows GHGPBTs below 10 years in some of these countries, mainly in France. Fig. 8 shows white regions for locations where the GHGPBT exceeds 10 years.

Fig. 9 shows the variation of the obtained results (for annual yield, PR_{AC}, EPBT and GHG emission factor) for all locations, in order to generally compare the different module technologies. Shown here is the very large variation in annual yield, EPBT and GHG emission factors, as these parameters are largely dependent on the geographical irradiance variation. The distribution of GHG emission factors is more or less a mirror image of the annual yield distribution, although the distributions in the figure are visually compressed. This is due to the large differences in the GHG emissions from manufacturing the respective technologies. The distributions of EPBT show more irregularities, due to the differences in grid efficiency from country to country. The variation in PR_{AC} is much smaller, as this parameter is corrected for irradiance, the biggest source of variation in PV performance.

The plots indicate that around or over 50% of the locations have an annual yield above 1500 kW h kW_p^{-1} y^{-1}, for all module technologies, except for CIGS modules, where the mean annual yield

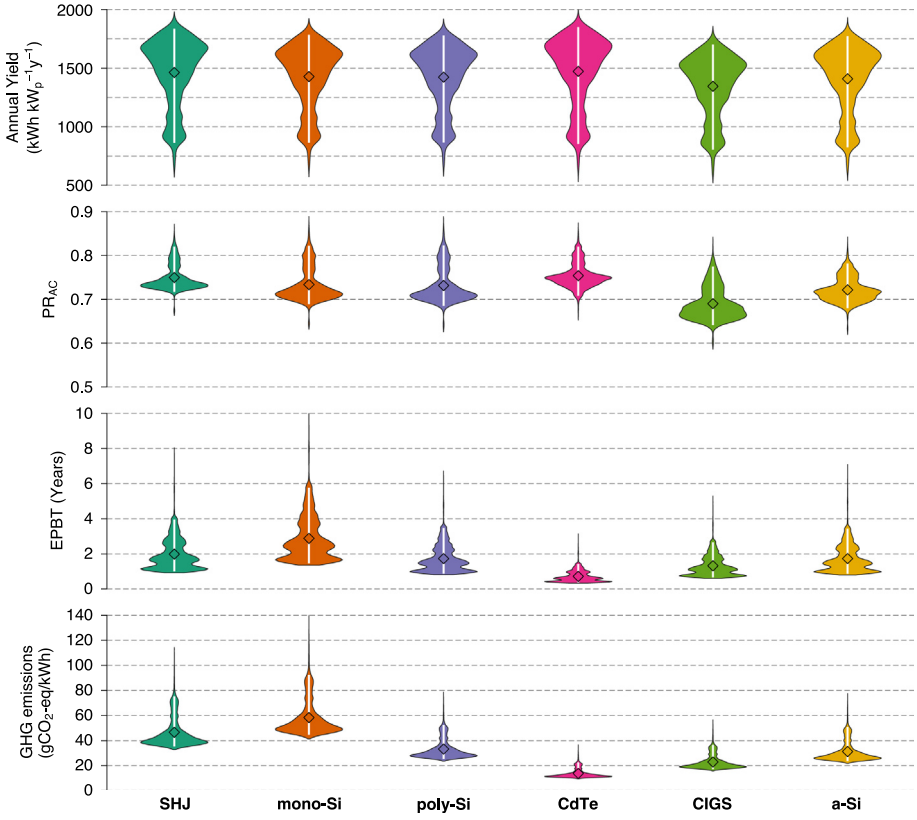

Fig. 9. Plots indicating the distribution of the obtained results, per technology, for all locations and modules, for annual yield, DC performance ratio, energy payback time (EPBT) and GHG emission factor. The diamond shaped markers indicate the overall means. The white lines indicate the range of 95% of the results around the median.

is above 1500 kW h kW_p^{-1} y^{-1} for only 35% of the locations. For all technologies the majority of locations show GHG emission factors below 60 gCO_2-eq/kW h, and EPBT below 3 years. For mono-Si and SHJ, the GHG emission factor is below 60gCO_2-eq/kW h in 71% and 84% of locations respectively, while for the other technologies this is for 99–100% of locations. EPBT of mono-Si and SHJ is below 3 years in 65% and 87% of all locations respectively, for the other technologies this figure is at least 93%. The distribution of PR_{AC} results for the poly-Si, CIGS and a-Si indicate that there is larger variation within the technology module groups, indicate by a slightly wider distribution. This is largely due to the stronger effect of temperature on the PR_{AC} of these module types.

4. Comparison of specific locations

Fig. 10 shows a comparison of the annual energy yield PR_{AC}, EPBT and GHG emission factors of the six studied module technologies in different specific locations around the globe: (1) Utrecht, a city in the center of the Netherlands representative for north-western Europe, (2) Seville, a city in the south of Spain representative for southern Europe, (3) Aouzou, a village in Chad in the central Sahara, and (4) Kinshasa and Brazzaville, two directly adjacent capital cities of the DR Congo and Congo respectively, in the tropics of central Africa, representing north-western European, southern European, desert and tropical climates, respectively.

The annual energy yield is highest for the modules in the Sahara which has a very high annual insolation (see Fig. 1), and relatively low for the location in NW Europe. Although the southern European location is of much higher latitude compared to the tropics location, the annual yield is much higher, as this location is semi-arid, with a low degree of cloud cover. The figure also indicates the variation (min–max range) of performance modelled for each module type and location. It indicates that especially for the Sahara and Tropics location, the variation of modelled performance is significant, especially for the poly-Si and CIGS modules. The SHJ systems have the highest annual energy yield at the NW Europe location, but are slightly outperformed by the CdTe systems at the other locations. The CIGS systems have lowest performance at all locations.

The performance ratio in Fig. 10 of the six module technologies shows that the relative performance (yield relative to annual insolation) is highest for the north-western European location, and is around 0.83 for most technologies, but lower for CIGS and a-Si. The lowest PR_{AC} is found in the tropical location, which is characterised by high operating temperatures and a high degree of cloud cover. High operating temperatures also significantly decrease the PR_{AC} for the southern European and Saharan locations.

The energy payback time shown in the third row of Fig. 10 shows that for at every location the lowest EPBT was found for the CdTe systems, while the mono-Si systems have the highest EPBT. For all four locations and six module technologies, the EPBT is below 4 years, while the EPBT for the CdTe systems is below 1 year in all locations. The CIGS modules have a relatively low EPBT despite the relatively low performance. The greenhouse gas emission factors in the bottom row of Fig. 10 show very similar trends compared to the EPBT graphs. The emissions attributed to PV electricity are much higher in the NW Europe location compared to the other locations, and the emission factors are lowest for CdTe systems, and highest for the mono-Si systems.

To investigate the effect of varying module surface tilt and orientation, we show in Fig. 11 how the POA irradiance and yield varies from its optimum value. Considering the effect of varying tilt and orientation is very similar for all technologies (see Fig. D.4 in the appendix), we present these results as averages for all technologies. The figure indicates that the tilt and orientation of the

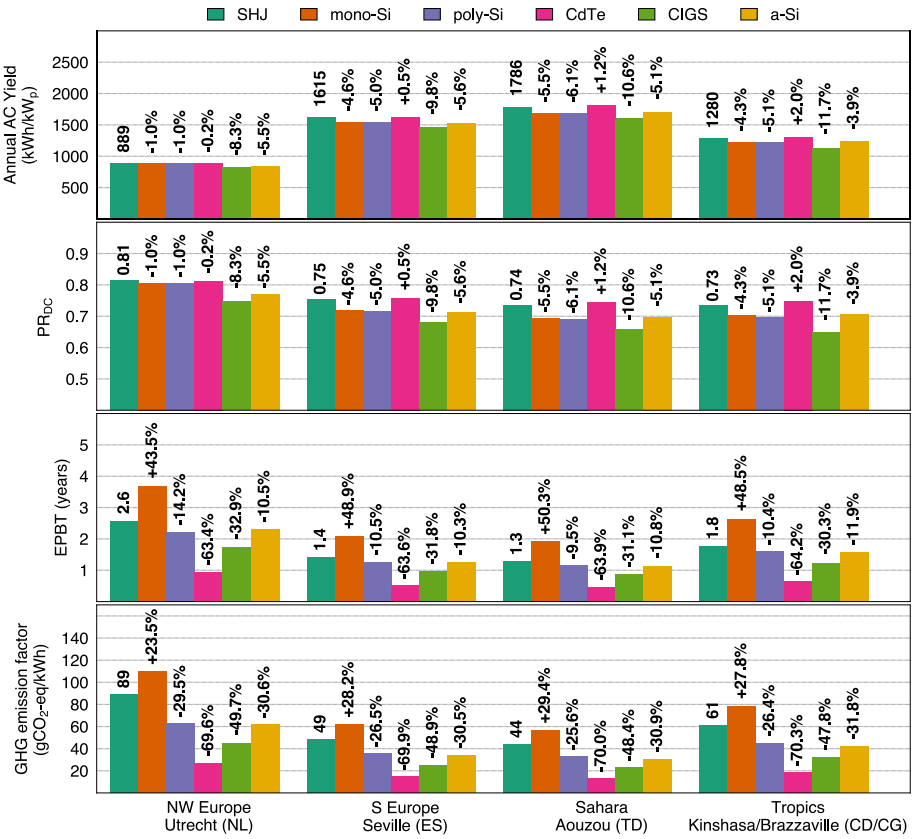

Fig. 10. Average annual yield, performance ratio, energy payback time and GHG emission factor of the six module technologies at four specific locations.

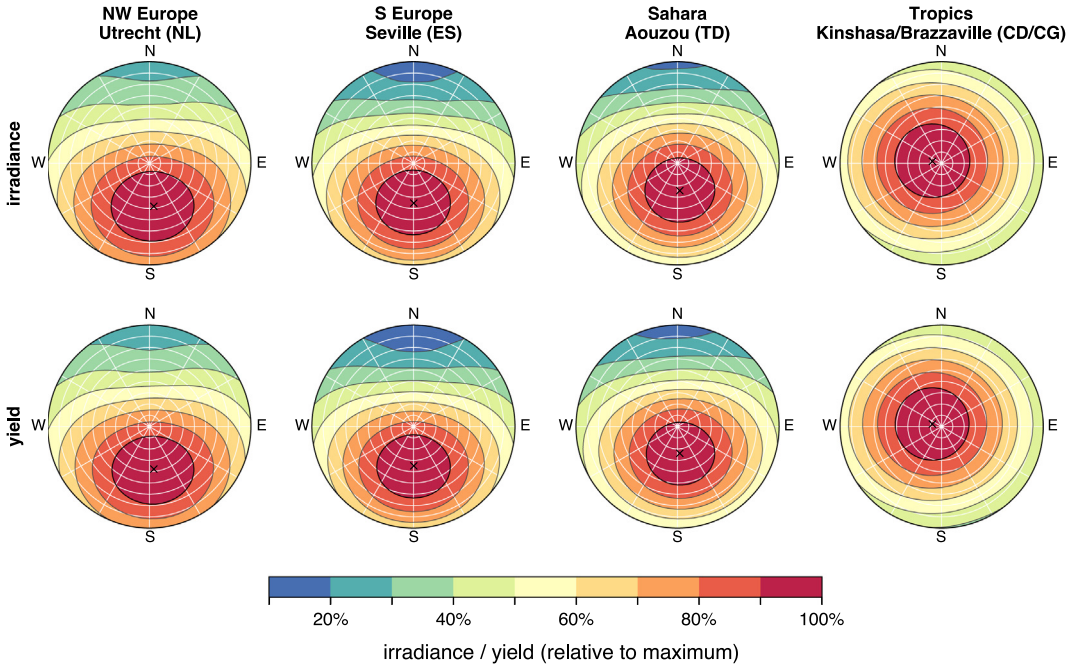

Fig. 11. Polar contour plot showing the effect of orientation and tilt on the global plane-of-array insolation (top row) and yield (bottom row) at 4 specific locations. The radius shows model inclination from 0 to 90 degrees, while the polar angle show module orientation. The black crosses indicate the tilt and orientation with highest irradiance and yield. The dark red areas indicate the tilt/orientation combination for which 90% of maximum irradiance is received or yield is generated. The yield results are averages over all the technologies. As shown in Fig. D.4, the effect of tilt and orientation on yield is very similar for all studied PV module technologies. (For interpretation of the references to colour in this figure legend, the reader is referred to the web version of this article.)

Table 2
Overview of the ranges over which tilt and orientation of the PV module surface can vary to achieve at minimum 90% of the optimum yield.

Location	Tilt range	Orientation range
NW Europe	8–69°	125–230°
SW Europe	6–63°	130–230°
Sahara	0–52°	100–250°
Tropics	0–41°	0–360°

PV modules surfaces can vary quite substantially without severely reducing the annual yield that can be achieved. In Table 2 we show how much tilt and orientation can change if the yield should remain at least 90% of the optimum value. Within these ranges, EPBT, GHG emission factor and GHGPBT would increase with maximum 11%. For example the EPBT of SHJ systems would increase to 2.9 and 1.6 years in North-West Europe and South-West Europe, respectively.

5. Discussion

In this paper we presented an analysis of the performance of PV systems, at optimal inclination and south orientation, based on different module technologies, to show the geospatial variation in performance, in terms of energy yield and energy payback time, carbon footprint and greenhouse gas payback time. Our results indicate that there is considerable variation of PV energy yield between module technologies, and considerable geographical variation in energy yield for all PV technologies. The latter variation is not only due to variations in the available solar irradiance at different locations, but also due to variations in operating conditions, mainly temperature.

Out of the six studied module technologies, cadmium telluride (CdTe) based systems seem to offer the best energy yield, and lowest environmental impact, in most locations, while the results of our modelling indicate that CIGS based systems show lower energy performance compared to the other module types over a broad geographical range. The results furthermore indicate that compared to conventional crystalline silicon modules (mono and poly), silicon heterojunction based systems offer on average 4–5% higher energy performance, mainly due the smaller detrimental effect elevated operating temperature has on its power output. Especially at lower latitudes, the energy performance of SHJ modules is higher (7–8%) compared to mono- and poly-crystalline silicon based systems.

In terms of environmental impact, all module types show that they have payback times around or well below 5 years, in terms of energy and greenhouse gas emissions, for most locations. At locations with low irradiance and/or locations with an efficient electricity grid or grids with high shares of renewable electricity, energy payback times are approaching ten years, while in some locations with very low grid emission factors, greenhouse gas payback times are over ten years. At maximum, the EPBT is 13.3 years for mono-Si systems at the Northern extreme of the investigated geographical scope. The 99th percentile however is only 6.7 years.The greenhouse gas emission factors of all technologies is however below 120 gCO_2-eq/kW h for nearly all locations, and below or around 50 gCO_2-eq/kW h for a broad geographical range. The environmental impact results are based on a life cycle assessment study that analysed typical or average modules for each technology, and thus not necessarily represent any specific PV module of the same technology. Also, as is shown in de Wild-Scholten (2013), the production location, or rather the source of electricity used during production, has a pronounced effect on the environmental performance of PV.

A large part of the variation in the performance of PV at different locations can be attributed to variation in operating temperature. For a-Si systems, with the lowest temperature coefficient, on average 41% of the variation of performance is due to variation in operating temperature. For the other technologies, this figure is

much higher at 67–70%. The temperatures modelled for the rooftop systems are higher compared to what would be modelled for open rack systems, so our results do not necessarily give a very accurate approximation of large-scale ground-mounted PV systems.

The results we have calculated here are based on assumed system losses, optimally oriented PV modules, and a yearly degradation rate of 0.67% for all studied module technologies. In practice, system losses, for instance due to soiling, shading, cabling and inverter losses could be higher. Furthermore, as mentioned in Section 2.4, research has shown that some technologies can have lower degradation rates than assumed here, while others exhibit higher degradation rates (Jordan et al., 2016). Would we have implemented the degradation rates shown in this study by Jordan et al., the results would be significantly affected, resulting in highest energy performance for mono-Si an poly-Si based systems, much lower performance for the SHJ, a-Si and especially CdTe based systems, and slightly higher energy performance for the CIGS based system.

In terms of module inclination, we have only considered the optimal module inclination for all locations. Whereas in some countries, like the Netherlands, the typical roof inclination of residential buildings is nearly equal to the optimal module inclination, this would likely not be the case in many other countries. Especially in locations with high fractions of direct irradiance, suboptimal module inclinations could significantly decrease the annual energy yield. In Fig. 11 we show the effect of varying both the inclination and orientation of the PV modules. The figure shows that for both irradiance and yield, inclination and orientation of the PV modules can vary quite significantly before the received irradiance and achieved yield drops below 90% of the maximum.

The calculation of the geographical variation of energy payback time and GHG emissions was performed based on a study by De Wild-Scholten from 2013 (de Wild-Scholten, 2013), and a study by the authors from 2015 (Louwen et al., 2015). Although more recent LCA studies are available, these two studies were chosen because the study by De Wild-Scholten presents results for all technologies except for SHJ, and the study we performed in 2015 is as of yet the only LCA study of SHJ based PV systems in peer-reviewed literature. Both studies do not include end-of-life treatment of the PV systems, which could lead to either under- or overestimation of the baseline environmental impact of PV systems. End-of-life treatment inherently would cost energy, however, by reclaiming energy intensive materials, benefits could be obtained. In a review of PV LCA, it was shown that although a very limited number of studies analysed decommissioning of PV systems ($n = 2$), decommissioning results in a net lowering (-3.3% for GHG emissions) of environmental impact (Nugent and Sovacool, 2014). A recent study quantified the environmental impact of recycling PV modules, and found that the energy impact of recycling 1000 kg of silicon PV modules would be 2780 MJ (Latunussa et al., 2016), roughly corresponding with 200 MJ_P/kW_p[3] , or about 1–2% of the total environmental impact of the module technologies studied here. This study however explicitly excludes any benefits of reclaimed materials. Other parameters not included in the analysis of environmental impact are transport, installation and operation of the PV systems. Our previous work showed that these phases in the life cycle have little to no effect on the total environmental footprint (Louwen et al., 2015).

The comparison of the six PV module technologies is based on performance modelling of eight types of modules for each technology, and the results for each technology are based on the average performance of these eight modules. For some technologies, there is considerable variation between the eight analysed modules, while for other technologies this variation is very limited. Fig. D.2 shows the variation (standard deviation) of the modelled annual energy yields for the different module sets. Especially the results for CdTe, CIGS and a-Si show higher standard deviation compared to the other module sets, for a-Si especially at high-irradiance locations. For, mono-Si, poly-Si and especially SHJ, the results of the eight studied modules are however very similar (low standard deviation). For SHJ this is likely due to the fact that all studied modules are from the same supplier, as there is a very limited amount of producers making SHJ modules. For the mono-Si and poly-Si modules there is more variation in the manufacturers, but we assume that variation here is limited due to these technologies being very mature.

[3] Assuming a PV module to have a weight of 20 kg and to have a rated power output of 275 W_p

6. Conclusions

Using the open source PV performance modelling tool PVlib-python, we modelled the performance of six different types of PV modules. Datasets of global horizontal irradiance, air temperature and wind speed, were used as inputs for the Sandia Array Performance Model. The datasets and model results cover a broad geographical range including most of Europe, Africa and the Middle-East. Finally, the model results were combined with results from LCA studies of PV systems to calculate the environmental footprint of the studied PV module technologies over the described geographical range.

Our results indicate that for most locations, cadmium telluride based PV systems offer the highest energy performance, although the difference with silicon heterojunction based PV systems is small (within 1% yield difference). The difference with mono-Si, poly-Si and a-Si based systems is larger, which have a 5% lower yield on average compared to CdTe, and 4–5% lower yield compared to SHJ systems. In our modelling results, especially CIGS modules show considerably lower performance (on average 5–10% lower in terms of annual electricity yield) compared to the other types of PV modules, over broad geographical ranges. When correcting for irradiance, energy performance of all module types was shown to have strong predominantly latitudinal variation, mainly due to differences in operating temperature. Annual yields of up to around 1800 kW h kW_p^{-1} y^{-1} are attained in very sunny locations, while in North-West Europe yields of around 900 kW h kW_p^{-1} y^{-1} are shown.

In terms of environmental impact the differences between the module types are greater, as the production of especially monocrystalline silicon wafer based PV modules is much more energy and greenhouse gas intensive than the production of thin film PV modules. As a result, the CdTe modules have lowest energy payback times (EPBT) and GHG emission factors. For all PV module technologies however, EPBT is below 3 years and GHG emission factors are below or around 50 gCO_2-eq/kW h for large geographical ranges, when installations are at optimal inclination and orientation.

Acknowledgements

This research was funded by Stichting Technologische Wetenschappen within the FLASH *Perspectief* programme under project number 12172.

Appendix A. Input LCA data

See Table A.1.

Table A.1
Overview of the LCA input parameters used in this study for calculating the energy payback time, non-renewable energy payback time, GHG emission factor and GHG payback time of PV systems based on the six PV technologies.

Module technology	Production in EU		Production in China		Assumed market average	
	GHG footprint (gCO_2-eq/kW_p)	CED (MJ_p/kW h)	GHG footprint (gCO_2-eq/kW_p)	CED (MJ_p/kW h)	GHG footprint (gCO_2-eq/kW_p)	CED (MJ_p/kW h)
SHJ[a]	1107	18589	2401	22237	1948	20960
mono-Si[b]	1280	26200	2870	31700	2314	29775
poly-Si[b]	824	15800	1590	18900	1322	17815
CdTe[b]	469	7290	630	7860	574	7661
CIGS[b]	715	12900	958	12900	873	12900
a-Si[b]	1020	17800	1360	17700	1241	17735

[a] Data from Louwen et al. (2015).
[b] Data from de Wild-Scholten (2013).

Appendix B. Description of the specific locations investigated

See Table B.1.

Table B.1
Overview of parameters describing the four specific locations investigated in this study.

Location	Coordinates	Annual insolation H_{POA} (kW h/m^2)	Mean annual air temperature (°C)
NW Europe	52°N 5°E	1146	10.5
SW Europe	37°5′N 6°W	2232	18.5
Sahara	21°5′N 17°E	2538	22.1
Tropics	4°5′S 15°E	1821	24.7

Appendix C. Input data for country GHG factor and grid efficiency

See Table C.2.

Table C.2
Overview of input data for GHG factor and grid efficiency.

Country	GHG/kW h	MJ_p/kW h	Note
Afghanistan	686	8.25	η_G, GHG[1]
Albania	686	3.85	GHG[1]
Algeria	836	11.10	
Andorra	382	8.25	η_G
Angola	435	4.81	
Armenia	184	7.43	
Austria	312	4.58	
Azerbaijan	637	9.91	
Belarus	1161	11.02	
Belgium	316	9.67	
Benin	736	12.11	
Bosnia and Herzegovina	1138	6.42	
Botswana	1423	12.19	GHG[2]
Bulgaria	709	9.27	
Burkina Faso	686	8.25	η_G, GHG[1]
Burundi	686	8.25	η_G, GHG[1]
Cameroon	311	4.76	
Central African Republic	686	8.25	η_G, GHG[1]
Chad	686	8.25	η_G, GHG[1]
Congo	260	5.33	
Congo, The Democratic Republic of the	686	3.86	GHG[1]
Côte d'Ivoire	545	7.75	
Croatia	560	5.08	
Czech Republic	764	10.23	
Denmark	584	6.68	
Djibouti	686	8.25	η_G, GHG[1]
Egypt	551	9.73	
Equatorial Guinea	686	8.25	η_G, GHG[1]
Eritrea	877	12.11	
Estonia	1184	5.46	
Ethiopia	686	3.88	GHG[1]
Finland	358	7.01	
France	112	9.16	
Gabon	471	6.55	
Gambia	686	8.25	η_G, GHG[1]
Georgia	133	4.36	
Germany	606	8.41	
Ghana	262	4.24	
Greece	846	8.12	
Guinea	686	8.25	η_G, GHG[1]
Guinea-Bissau	686	8.25	η_G, GHG[1]
Hungary	497	10.46	
Iran, Islamic Republic of	732	10.31	
Iraq	980	9.60	
Ireland	485	8.25	
Israel	867	11.55	
Italy	496	6.78	
Jordan	705	11.85	
Kazakhstan	1423	10.30	GHG[2]
Kenya	241	5.10	
Kosovo	686	11.65	GHG[1]
Kuwait	1117	11.82	
Latvia	343	5.47	
Lebanon	806	10.70	
Lesotho	686	8.25	η_G, GHG[1]
Liberia	686	8.25	η_G, GHG[1]
Libya	638	11.56	
Lithuania	981	6.85	
Luxembourg	296	8.35	
Macedonia, Republic of	959	7.77	
Madagascar	686	8.25	η_G, GHG[1]
Malawi	686	8.25	η_G, GHG[1]
Mali	686	8.25	η_G, GHG[1]
Mauritania	686	8.25	η_G, GHG[1]
Moldova, Republic of	1423	9.86	GHG[2]
Montenegro	573	5.13	
Morocco	767	9.19	
Mozambique	686	3.91	GHG[1]
Namibia	686	3.97	GHG[1]
Netherlands	658	9.64	
Niger	686	12.03	GHG[1]
Nigeria	845	8.27	
Norway	85	3.91	
Oman	949	11.19	
Pakistan	174	7.12	
Palestine, State of	686	8.25	η_G, GHG[1]
Poland	1097	10.25	
Portugal	433	5.67	
Qatar	1423	11.16	GHG[2]
Romania	735	7.10	
Russian Federation	994	8.62	
Rwanda	686	8.25	η_G, GHG[1]
Saudi Arabia	837	11.48	

Table C.2 (*continued*)

Country	GHG/kW h	MJ_p/kW h	Note
Senegal	734	10.05	
Serbia	901	7.79	
Sierra Leone	686	8.25	η_G, GHG[1]
Slovakia	484	8.39	
Slovenia	401	7.27	
Somalia	686	8.25	η_G, GHG[1]
South Africa	972	12.05	
South Sudan	221	12.15	
Spain	382	6.98	
Sudan	221	4.43	
Swaziland	686	8.25	η_G, GHG[1]
Sweden	62	5.78	
Switzerland	54	5.35	
Syrian Arab Republic	691	9.33	
Tanzania, United Republic of	487	7.09	
Togo	686	4.33	GHG[1]
Tunisia	482	10.77	
Turkey	545	7.40	
Turkmenistan	1421	11.16	
Uganda	686	8.25	η_G, GHG[1]
Ukraine	753	10.52	
United Arab Emirates	664	11.17	
United Kingdom	603	9.47	
Uzbekistan	813	7.97	
Western Sahara	767	8.25	η_G
Yemen	826	11.87	
Zambia	686	3.86	GHG[1]
Zimbabwe	387	5.68	

η_G: Using average grid efficiency due to missing grid efficiency data.
GHG[1]: Using average GHG factor because of missing GHG data.
GHG[2]: Outlier GHG factor restricted to 95th percentile.

Appendix D. Supporting figures

See Figs. D.1–D.4.

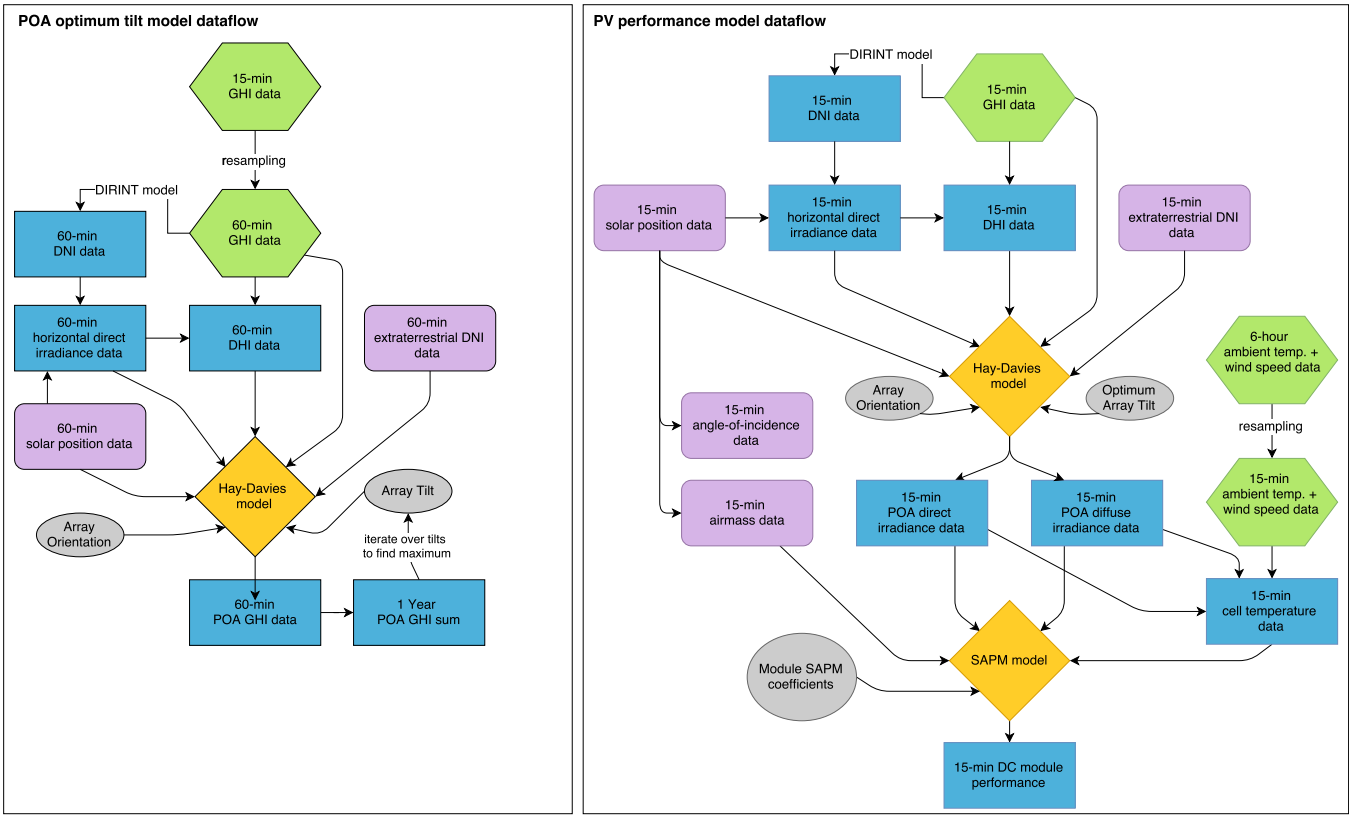

Fig. D.1. Dataflow for the determination of global irradiance optimum plane-of-array tilt (left) and the modelling of PV module power output (right).

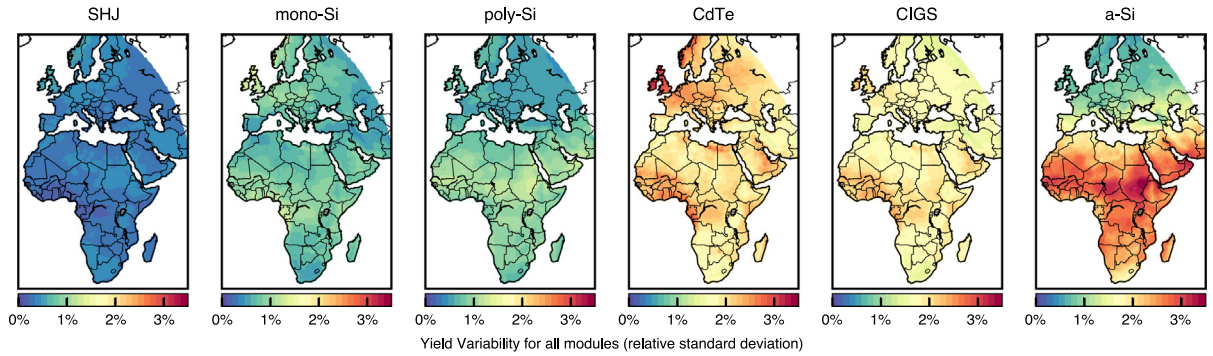

Fig. D.2. Overview of the variation of modelled annual yield between the eight modelled PV modules for each technology. The figures represent the standard deviation, relative to the mean at each location.

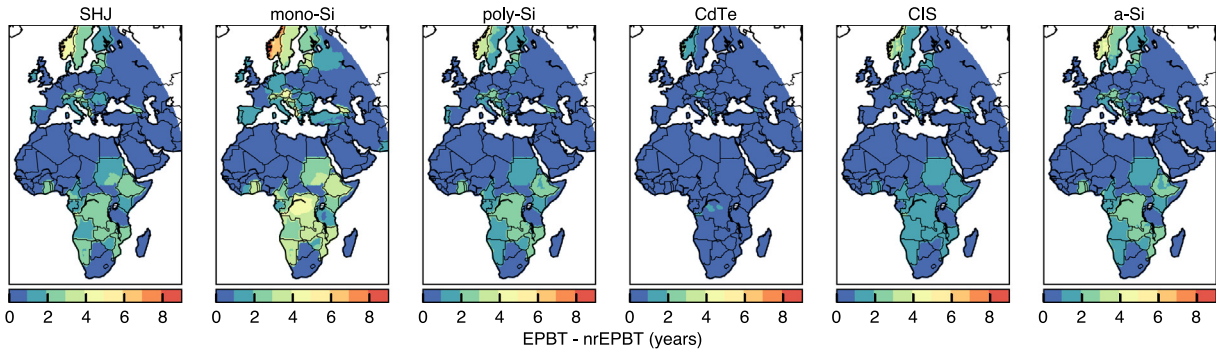

Fig. D.3. Overview of the difference between standard Energy Payback Time (EPBT) and non-renewable Energy Payback Time (nrEBPT) of optimally tilted PV systems in years, calculated with the Sandia Array Performance Model (King et al., 2004) using 15-min resolution plane-of-array irradiance time series (SoDa, 2016) and 6-h ambient temperature and wind-speed time series (European Centre for Medium-Range Weather Forecasts, 2016) for 2005.

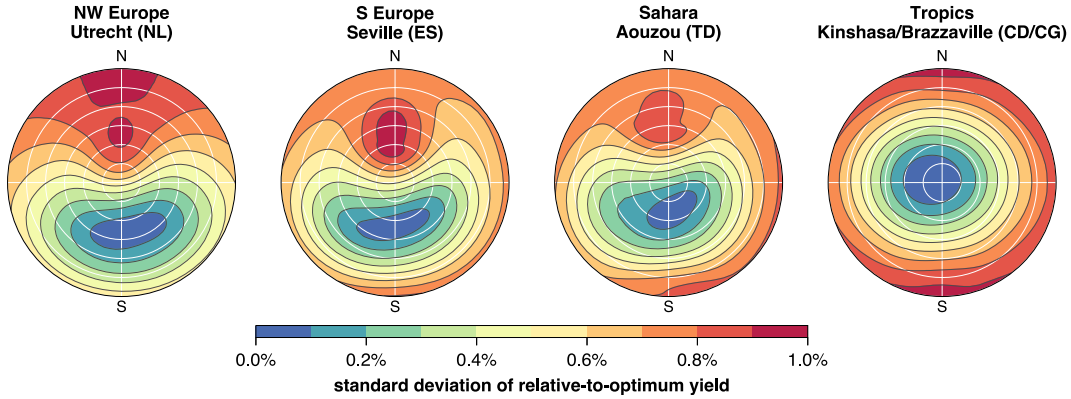

Fig. D.4. Variation of the effect of changing tilt and orientation between the six studied PV module technologies, calculated as the standard deviation of the yield relative to the optimum yield. The figures indicate that at maximum, the standard deviations of relative-to-optimum yield between the technologies approaches 1%.

References

Alsema, E.A., Fraile, D., Frischknecht, R., Fthenakis, V., Held, M., Kim, H.C., Pölz, W., Raugei, M., de Wild-Scholten, M., 2009. Methodology Guidelines on Life Cycle Assessment of Photovoltaic Electricity, Subtask 20 'LCA', IEA PVPS Task 12, by: Publication date: ECN Solar Energy 5-10-2009.

Bloomberg L.P., 2016. New Record Set for World's Cheapest Solar, Now Undercutting Coal. <http://www.bloomberg.com/news/articles/2016-05-03/solar-developers-undercut-coal-with-another-record-set-in-dubai>.

Breyer, C., Gerlach, A., 2013. Global overview on grid-parity. Prog. Photovoltaics Res. Appl. 21 (1), 121–136. http://dx.doi.org/10.1002/pip.1254.

Corcelli, F., Ripa, M., Leccisi, E., Cigolotti, V., Fiandra, V., Graditi, G., Sannino, L., Tammaro, M., Ulgiati, S., 2016. Sustainable urban electricity supply chain – indicators of material recovery and energy savings from crystalline silicon photovoltaic panels end-of-life, Ecol. Indic. http://dx.doi.org/10.1016/j.ecolind.2016.03.028.

de Wild-Scholten, M.J., 2013. Energy payback time and carbon footprint of commercial photovoltaic systems. Sol. Energy Mater. Sol. Cells 119, 296–305. http://dx.doi.org/10.1016/j.solmat.2013.08.037.

Dobos, Aron P., 2014. PVWatts Version 5 Manual. Tech. Rep. NREL/TP-6A20-62641, NREL.

Duffie, J.A., Beckman, W.A., 2013. Solar Engineering of Thermal Processes. Wiley, New York. oCLC: 934630622.

European Centre for Medium-Range Weather Forecasts, 2016. Public Datasets. <http://apps.ecmwf.int/datasets/>.

First Solar, 2016. First Solar Series 5 Modules—First Solar. <http://www.firstsolar.com/Technologies-and-Capabilities/PV-Modules/First-Solar-Series-5-Modules>.

Fraunhofer ISE, 2016. Photovoltaics Report. Tech. Rep., Fraunhofer ISE, Freiburg, Germany.
Frischknecht, R., Heath, G., Raugei, M., Sinha, P., de Wild-Scholten, M., January 2016. Methodology Guidelines on Life Cycle Assessment of Photovoltaic Electricity, third ed. Tech. Rep. IEA-PVPS T12-08:2016. International Energy Agency Photovoltaic Power Systems Programme.
Fthenakis, V., Frischknecht, R., Raugei, M., Kim, H., Alsema, E., Held, M., de Wild-Scholten, M., November 2011. Methodology Guidelines on Life Cycle Assessment of Photovoltaic Electricity, second ed. Tech. Rep. IEA-PVPS T12-03:2011. IEA Photovoltaic Power Systems Programme.
García, M., Marroyo, L., Lorenzo, E., Pérez, M., 2011. Soiling and other optical losses in solar-tracking PV plants in Navarra. Prog. Photovoltaics Res. Appl. 19 (2), 211–217. http://dx.doi.org/10.1002/pip.1004.
Haegel, N.M., Margolis, R., Buonassisi, T., Feldman, D., Froitzheim, A., Garabedian, R., Green, M., Glunz, S., Henning, H.-M., Holder, B., Kaizuka, I., Kroposki, B., Matsubara, K., Niki, S., Sakurai, K., Schindler, R.A., Tumas, W., Weber, E.R., Wilson, G., Woodhouse, M., Kurtz, S., 2017. Terawatt-scale photovoltaics: trajectories and challenges. Science 356 (6334), 141–143. http://dx.doi.org/10.1126/science.aal1288.
Hansen, Clifford W., Stein, Joshua S., Riley, Daniel., 2012. Effect of Time Scale on Analysis of PV System Performance. Sandia National Laboratories.
Hay, J.E., Davies, J.A., 1980. Calculation of the solar radiation incident on an inclined surface. In: Proc. of First Canadian Solar Radiation Data Workshop (Eds: JE Hay and TK Won), Ministry of Supply and Services Canada, vol. 59.
Holmgren, W.F., Andrews, R.W., Lorenzo, A.T., Stein, J.S., 2015. PVLIB python 2015. In: Photovoltaic Specialist Conference (PVSC), 2015 IEEE 42nd. IEEE, pp. 1–5.
IEA PVPS, 2015. Trends 2015 in Photovoltaic Applications. Tech. Rep. IEA-PVPS T1-27:2015. International Energy Agency.
IEA PVPS, 2016. A Snapshot of Global PV (1992–2015). Tech. Rep., IEA Photovoltaic Power Systems Programme.
IEC TS 61724-3:2016, 2016. Photovoltaic System Performance – Part 3: Energy Evaluation Method.
Ineichen, P., Perez, R.R., Seal, R.D., Maxwell, E.L., Zalenka, A., 1992. Dynamic global-to-direct irradiance conversion models. ASHRAE Trans. 98 (1), 354–369.
ISO 14040:2006, 2016. Environmental Management – Life Cycle Assessment – Principles and Framework. International Organization for Standardization (ISO), Geneva, Switzerland.
ISO 14044:2006, 2016. Life Cycle Assessment – Requirements and Guidelines. Tech. Rep. International Organization for Standardization (ISO), Geneva, Switzerland.
ITRPV, 2017. International Technology Roadmap for Photovoltaic (ITRPV) – 2016 Results. Tech. Rep..
Jean, J., Brown, P.R., Jaffe, R.L., Buonassisi, T., Bulović, V., 2015. Pathways for solar photovoltaics. Energy Environ. Sci. 8 (4), 1200–1219. http://dx.doi.org/10.1039/C4EE04073B.
Jordan, D.C., Kurtz, S.R., VanSant, K., Newmiller, J., 2016. Compendium of photovoltaic degradation rates: photovoltaic degradation rates. Prog. Photovoltaics Res. Appl. 24 (7), 978–989. http://dx.doi.org/10.1002/pip.2744.
Jungbluth, N., Stucki, M., Frischknecht, R., 2009. Photovoltaics. In: Dones, R. (Ed.), Sachbilanzen von Energiesystemen: Grundlagen Für Den Ökologischen Vergleich von Energiesystemen Und Den Einbezug von Energiesystemen in Ökobilanzen Für Die Schweiz. Ecoinvent Report No. 6-XII, no. 6, Swiss Centre for Life Cycle Inventories, Dübendorf, Switzerland.
KANEKA Solar Energy, 2016. Why Thin-Film Silicon? Technology KANEKA Solar Energy. <http://www.kaneka-solar.com/>.
King, D.L., Boyson, W.E., Kratochvill, J.A., 2004. Photovoltaic Array Performance Model. Tech. Rep. SAND2004-3535, Sandia National Laboratories, Albuquerque, New Mexico, USA.
Latunussa, C.E.L., Ardente, F., Blengini, G.A., Mancini, L., 2016. Life cycle assessment of an innovative recycling process for crystalline silicon photovoltaic panels. Sol. Energy Mater. Sol. Cells 156, 101–111. http://dx.doi.org/10.1016/j.solmat.2016.03.020.
Leccisi, E., Raugei, M., Fthenakis, V., 2016. The energy and environmental performance of ground-mounted photovoltaic systems – a timely update. Energies 9 (8), 622. http://dx.doi.org/10.3390/en9080622.
Louwen, A., van Sark, W.G.J.H.M., Schropp, R.E.I., Turkenburg, W.C., Faaij, A.P.C., 2015. Life-cycle greenhouse gas emissions and energy payback time of current and prospective silicon heterojunction solar cell designs. Prog. Photovoltaics Res. Appl. 23 (10), 1406–1428. http://dx.doi.org/10.1002/pip.2540.
Louwen, A., van Sark, W.G.J.H.M., Faaij, A.P.C., Schropp, R.E.I., 2016. Re-assessment of net energy production and greenhouse gas emissions avoidance after 40 years of photovoltaics development. Nat. Commun. 7, 13728. http://dx.doi.org/10.1038/ncomms13728.
Louwen, A., de Waal, A.C., Schropp, R.E.I., Faaij, A.P.C., van Sark, W.G.J.H.M., 2017. Comprehensive characterisation and analysis of PV module performance under real operating conditions: comprehensive characterisation and analysis of PV module performance under real operating conditions. Prog. Photovoltaics Res. Appl. 25 (3), 218–232. http://dx.doi.org/10.1002/pip.2848.
Makrides, G., Zinsser, B., Schubert, M., Georghiou, G.E., 2014. Performance loss rate of twelve photovoltaic technologies under field conditions using statistical techniques. Sol. Energy 103, 28–42. http://dx.doi.org/10.1016/j.solener.2014.02.011.
Nugent, D., Sovacool, B.K., 2014. Assessing the lifecycle greenhouse gas emissions from solar PV and wind energy: a critical meta-survey. Energy Policy 65, 229–244. http://dx.doi.org/10.1016/j.enpol.2013.10.048.
Paltridge, G.W., Platt, C.M.R., 1976. Radiative Processes in Meteorology and Climatology. Developments in Atmospheric Science, vol. 5. Elsevier, Amsterdam. oCLC: 2430889.
Panasonic Corporation, 2016. State of the Art Technology—Solar—Eco Solutions—Business—Panasonic Global. <http://panasonic.net/ecosolutions/solar/hit/>.
Pérez-López, P., Gschwind, B., Blanc, P., Frischknecht, R., Stolz, P., Durand, Y., Heath, G., Ménard, L., Blanc, I., 2016. ENVI-PV: an interactive web client for multi-criteria life cycle assessment of photovoltaic systems worldwide. Prog. Photovoltaics Res. Appl. http://dx.doi.org/10.1002/pip.2841. n/a–n/a.
Picault, D., Raison, B., Bacha, S., de la Casa, J., Aguilera, J., 2010. Forecasting photovoltaic array power production subject to mismatch losses. Sol. Energy 84 (7), 1301–1309. http://dx.doi.org/10.1016/j.solener.2010.04.009.
Reich, N.H., Mueller, B., Armbruster, A., van Sark, W.G.J.H.M., Kiefer, K., Reise, C., 2012. Performance ratio revisited: Is PR > 90% realistic? Prog. Photovoltaics Res. Appl. 20 (6), 717–726. http://dx.doi.org/10.1002/pip.1219.
Sharma, V., Kumar, A., Sastry, O.S., Chandel, S.S., 2013. Performance assessment of different solar photovoltaic technologies under similar outdoor conditions. Energy 58, 511–518. http://dx.doi.org/10.1016/j.energy.2013.05.068.
SoDa, 2016. SoDa – Free Time-series of Solar Radiation Data. <http://www.soda-is.com/eng/services/services_radiation_free_eng.php>.
Solar Frontier, 2016. Performance. <http://www.solar-frontier.com/eng/technology/Performance/index.html>.
Stion, 2016. Performance. <http://www.stion.com/products/performance/>.
United Nations Statistics Division, 2015. Energy Statistics Database. <http://data.un.org/>.
van Sark, W.G.J.H.M., Reich, N.H., Müller, B., Armbruster, K., Kiefer, K., Reise, C., 2012. Review of PV performance ratio development. In: World Renewable Energy Congress. Denver, CO, USA.
Wernet, G., Bauer, C., Steubing, B., Reinhard, J., Moreno-Ruiz, E., Weidema, B., 2016. The ecoinvent database version 3 (Part I): Overview and methodology. Int. J. Life Cycle Assess. 21 (9), 1218–1230. http://dx.doi.org/10.1007/s11367-016-1087-8.
Wetzel, T., Borchers, S., 2014. Update of energy payback time and greenhouse gas emission data for crystalline silicon photovoltaic modules: broader perspectives, Prog. Photovoltaics: Res. Appl. (in press). http://dx.doi.org/10.1002/pip.2548.
World Resources Institute, 2015. Climate Analysis Indicators Tool: WRI's Climate Data Explorer. <http://cait.wri.org>.
Zhao, J., Mehlich, H., Hausmann, J., Richter, M., Gruber, B., Weinke, M., Schorch, M., Kowalewski, J., Krause, J., Papet, P., Stein, W., Blanchet, M., Söderström, T., Richter, A., Beyer, S., Ufheil, J., 2013. Pilot Production of 6"-Heterojunction Cells and Modules at Meyer-Burger and Outdoor Performance. http://dx.doi.org/10.4229/28thEUPVSEC2013-2DV.3.19.
Zinsser, B., Makrides, G., Schubert, M., Georghiou, G., Werner, J., 2009. Temperature and Irradiance Effects on Outdoor Field Performance. http://dx.doi.org/10.4229/24thEUPVSEC2009-5BV.2.19.